

Two-Dimensional Analysis of the Power Transfer between Crossed Laser Beams

The indirect-drive approach to inertial confinement fusion¹ involves laser beams that cross as they enter the hohlraum. Ion-acoustic waves in the plasma at the overlap region can transfer power between the beams. Since this could adversely affect the implosion symmetry, it is important to understand the mechanisms that make such a transfer possible. In this context, two studies have been made of the interaction of crossed laser beams mediated by an ion-acoustic wave. Krueer *et al.*² performed a one-dimensional analysis of the steady-state power transfer, emphasizing the effects of different beam frequencies and the inhomogeneity of the plasma. Eliseev *et al.*³ performed two-dimensional simulations of the interaction of equal-frequency beams in a homogeneous plasma. In addition to observing a time-dependent power transfer between the beams, they observed several secondary processes and supplemented their numerical simulations with one-dimensional analyses of certain processes. Here, we present a two-dimensional analysis of the power transfer between beams of unequal frequency in a homogeneous plasma, for both the transient and steady-state regimes.

Governing Equations

Laser beams that cross interact via ion-acoustic waves in the irradiated plasma. The interaction geometry is shown in Fig. 66.30 and is governed by Maxwell's wave equation⁴

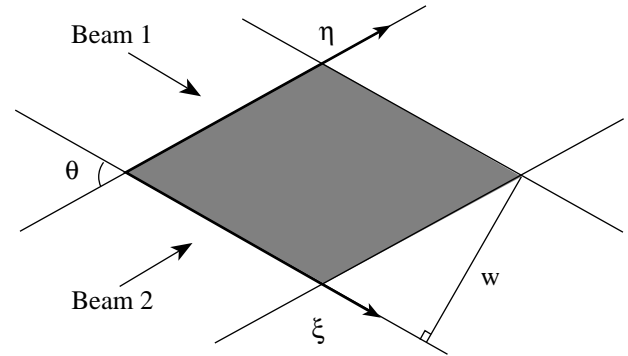
$$\left(\partial_{tt}^2 + \omega_e^2 - c^2 \nabla^2\right) A_h = -\omega_e^2 n_l A_h \quad (1)$$

for the electromagnetic potential together with the ion-acoustic (sound) wave equation⁴

$$\left(\partial_{tt} + 2v_s \partial_t - c_s^2 \nabla^2\right) n_l = \frac{1}{2} c_s^2 \nabla^2 \langle A_h^2 \rangle. \quad (2)$$

The electromagnetic potential $A_h = (v_h/c_s)(m_e/m_i)^{1/2}$ is the quiver velocity of electrons oscillating in the high-frequency electric field divided by a characteristic speed that is of the order of the electron thermal speed, n_l is the low-frequency electron-density fluctuation associated with the ion-acoustic

wave divided by the background electron density, and the $\langle \rangle$ signify that only the low-frequency response to the ponderomotive force was retained.



P1525

Figure 66.30
Geometry of the interaction of crossed laser beams. The beam widths are equal and denoted by w , and the beam intersection angle is denoted by θ . The characteristic coordinates ξ and η measure distance in the propagation directions of beams 1 and 2, respectively.

By substituting the Ansatz

$$A_h(\xi, \eta, t) = A_1(\xi, \eta, t) \exp[i(k_1 \xi - \omega_1 t)] + A_2(\xi, \eta, t) \exp[i(k_2 \eta - \omega_2 t)] + c.c. \quad (3)$$

and

$$n_l(\xi, \eta, t) = n(\xi, \eta, t) \exp[i(k_1 \xi - k_2 \eta)] + c.c. \quad (4)$$

into Eqs. (1) and (2), and making the slowly varying envelope approximation, one can show that

$$\partial_\xi A_1 = -i(\omega_e^2/2\omega_1 v_1) n A_2 \exp(i\omega t), \quad (5)$$

$$\partial_\eta A_2 = -i(\omega_e^2/2\omega_2 v_2) n^* A_1 \exp(-i\omega t),$$

and

$$(\partial_{tt} + 2v_s \partial_t + \omega_s^2)n = -\omega_s^2 A_1 A_2^* \exp(-i\omega t), \quad (6)$$

where v_1 is the group velocity of the higher-frequency beam; v_2 is the group velocity of the lower-frequency beam; $\omega = \omega_1 - \omega_2$ is the difference between the beam frequencies; $\mathbf{k}_s = \mathbf{k}_1 - \mathbf{k}_2$ is the ion-acoustic wave vector; and $\omega_s = c_s k_s$ is the ion-acoustic frequency. The characteristic variables ξ and η measure distance in the propagation directions of beams 1 and 2, respectively. The time derivatives were omitted from Eqs. (5) because the time taken for the laser beams to cross the interaction region is much shorter than the time taken for the ion-acoustic wave to respond to the ponderomotive force.

Steady-State Analysis

In steady state, the beams interact according to

$$\partial_\xi A_1 = (i\alpha - \beta)|A_2|^2 A_1, \quad (7)$$

$$\partial_\eta A_2 = (i\alpha + \beta)|A_1|^2 A_2,$$

where the nonlinear coefficients

$$\alpha = \frac{\omega_e^2 \omega_s^2 (\omega_s^2 - \omega^2)}{2\omega_2 v_2 \left[(\omega_s^2 - \omega^2)^2 + 4v_s^2 \omega^2 \right]}, \quad (8)$$

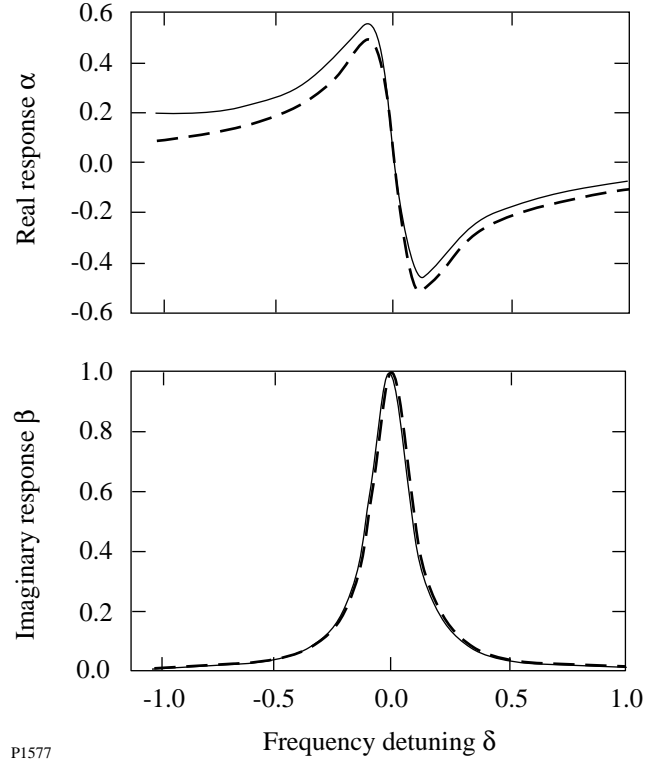
$$\beta = \frac{\omega_e^2 \omega_s^2 v_s \omega}{\omega_2 v_2 \left[(\omega_s^2 - \omega^2)^2 + 4v_s^2 \omega^2 \right]}.$$

Since $|\omega| \ll \omega_1$, the differences between ω_1 and ω_2 and v_1 and v_2 were neglected in the first of Eqs. (7).⁵ In the Lorentzian approximation

$$\alpha \approx \frac{-\omega_e^2 \omega_s \delta}{4\omega_2 v_2 (\delta^2 + v_s^2)}, \quad \beta \approx \frac{\omega_e^2 \omega_s v_s}{4\omega_2 v_2 (\delta^2 + v_s^2)}, \quad (9)$$

where the frequency-detuning parameter $\delta = \omega - \omega_s$. The coefficients α and β characterize the real and imaginary parts, respectively, of the ion-acoustic response to the ponderomotive force [see Eq. (6)]. They are plotted as functions of δ

in Fig. 66.31, for the case in which $v_s/\omega_s = 0.1$. Both coefficients are normalized to $\omega_e^2 \omega_s^2 / 4\omega_2 \omega_s v_2 v_s$, which, apart from a factor of $|A_1|^2$, is the spatial growth rate of stimulated Brillouin scattering (SBS) in the strong-damping limit. Although the Lorentzian approximation for α becomes less accurate as the magnitude of the frequency-detuning parameter increases, the Lorentzian approximation for β is accurate for arbitrary frequency detuning. For values of v_s/ω_s larger than 0.1, there are significant discrepancies between the approximate and exact expressions for both coefficients.



P1577

Figure 66.31

Nonlinear coefficients α and β [Eqs. (7)], normalized to the resonant gain coefficient, plotted as functions of the frequency detuning parameter δ/ω_s for the case in which $v_s/\omega_s = 0.1$. The coefficients α and β characterize the real and imaginary parts, respectively, of the ion-acoustic response to the ponderomotive force. The solid lines represent the exact coefficients [Eqs. (8)] and the dashed lines represent the approximate coefficients [Eqs. (9)].

Equations (7) are solved subject to the boundary conditions

$$A_1(0, \eta) = A_0, \quad A_2(\xi, 0) = \rho A_0, \quad (10)$$

where ρ is the ratio of the amplitudes of the incident beams. By changing variables according to

$$B_1 = A_1 \exp\left(-i\alpha \int_0^\xi |A_2|^2 d\xi'\right), \quad (11)$$

$$B_2 = A_2 \exp\left(-i\alpha \int_0^\eta |A_1|^2 d\eta'\right),$$

one can reduce Eqs. (7) to

$$\partial_\xi B_1 = -\beta |B_2|^2 B_1, \quad \partial_\eta B_2 = \beta |B_1|^2 B_2. \quad (12)$$

It is convenient to define the normalized intensities

$$I_1 = |B_1|^2 / |A_0|^2 \quad \text{and} \quad I_2 = |B_2|^2 / |A_0|^2,$$

the normalized distances

$$x = 2\beta |A_0|^2 \xi \quad \text{and} \quad y = 2\beta |A_0|^2 \eta,$$

and the normalized beam width

$$l = 2\beta |A_0|^2 w / \sin \theta,$$

where w is the physical beam width and θ is the beam intersection angle (see Fig. 66.30). In terms of these dimensionless variables, Eqs. (12) become

$$\partial_x I_1 = -I_2 I_1, \quad \partial_y I_2 = I_1 I_2 \quad (13)$$

and the boundary conditions [Eqs. (10)] become

$$I_1(0, y) = 1, \quad I_2(x, 0) = r, \quad (14)$$

where $r = |\rho|^2$ is the ratio of the beams' intensities.

Despite the fact that Eqs. (13) are nonlinear and describe beam propagation in two directions, there is a way to solve them analytically.^{6,7} It is convenient to define

$$P_1(x, y) = \int_0^y I_1(x, y') dy', \quad (15)$$

$$P_2(x, y) = \int_0^x I_2(x', y) dx'.$$

Physically, $P_1(x, l)$ is the power in the cross section of beam 1 that is a distance x from the entrance to the interaction region,

and $P_2(l, y)$ is the power in the cross section of beam 2 that is a distance y from the entrance to the interaction region. By combining Eqs. (13), one can show that

$$\partial_x P_1 = r [1 - \exp(P_1)], \quad (16)$$

from which it follows that

$$P_1(x, y) = -\log\{1 - \exp(-rx)[1 - \exp(-y)]\}. \quad (17)$$

It then follows from Eq. (17), and the relations $I_1 = \partial_y P_1$ and $I_2 = r \exp(P_1)$, that

$$I_1(x, y) = \frac{\exp(-y)}{\exp(rx) - 1 + \exp(-y)},$$

$$I_2(x, y) = \frac{r \exp(rx)}{\exp(rx) - 1 + \exp(-y)}. \quad (18)$$

By combining Eqs. (13), one can also show that

$$P_2(x, y) = \log\{1 + \exp(y)[\exp(rx) - 1]\}. \quad (19)$$

Equation (19) and the relations $I_2 = \partial_x P_2$ and $I_1 = \exp(-P_2)$ are consistent with solutions (18).

The beam-intensity profiles are displayed in Fig. 66.32, for the case in which $l = 3$ and $r = 0.01$. Notice that the intensity of beam 1 is nearly constant and the intensity of beam 2 is nearly independent of x . When $rl \ll 1$, as it is for Fig. 66.32, Eqs. (18) reduce to $I_1 \approx 1$ and $I_2 \approx r \exp(y)$ in agreement with the linearized versions of Eqs. (13).

The beam-intensity profiles are also displayed in Fig. 66.33, for the case in which $l = 3$ and $r = 0.1$. Notice that the intensity profiles are highly two-dimensional. Beam 1 is depleted as it propagates in the x direction, and beam 2 is amplified as it propagates in the y direction. Consequently, the depletion of beam 1 along the characteristic $y = l$ is more rapid than its depletion along the characteristic $y = 0$, and the amplification of beam 2 along the characteristic $x = 0$ is more rapid than its amplification along the characteristic $x = l$.

It follows from Eqs. (17) and (19) that

$$P_2(x, y) - P_2(x, 0) = P_1(0, y) - P_1(x, y); \quad (20)$$

the power gained by beam 2 must equal the power lost by beam 1. The power transfer $P_2(l, l) - P_2(l, 0)$ is denoted by $T(l)$ and is given by

$$T(l) = \log\{\exp(-rl) + \exp(l)[1 - \exp(-rl)]\}. \quad (21)$$

Since the normalized incident power is l , the fractional power transfer is $T(l)/l$. This fractional power transfer is plotted as a function of l in Fig. 66.34. It is not difficult to show that $T(l)/l \approx r[\exp(l) - 1]$ for $rl \ll 1$ and $l \sim 1$, and $T(l)/l \approx 1$ for $l \gg 1$.

Despite the complexity of the beam evolution, which is two-dimensional and nonlinear, the power transfer is characterized by two dimensionless parameters. The first, r , is simply the ratio of the incident beam intensities. The second, l , depends on several dimensional parameters that characterize the beams

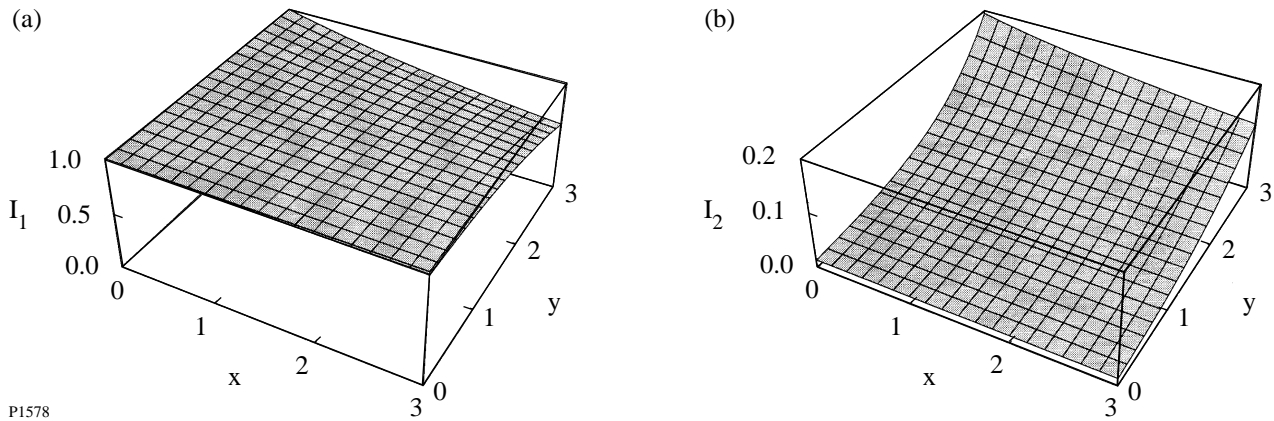


Figure 66.32 Beam-intensity profiles [Eqs. (18)] for the case in which the normalized beamwidth $l = 3$ and the ratio of the incident beam intensities $r = 0.01$. Notice that the intensity of beam 1 is nearly constant and the intensity of beam 2 is nearly independent of x , as linear theory predicts.

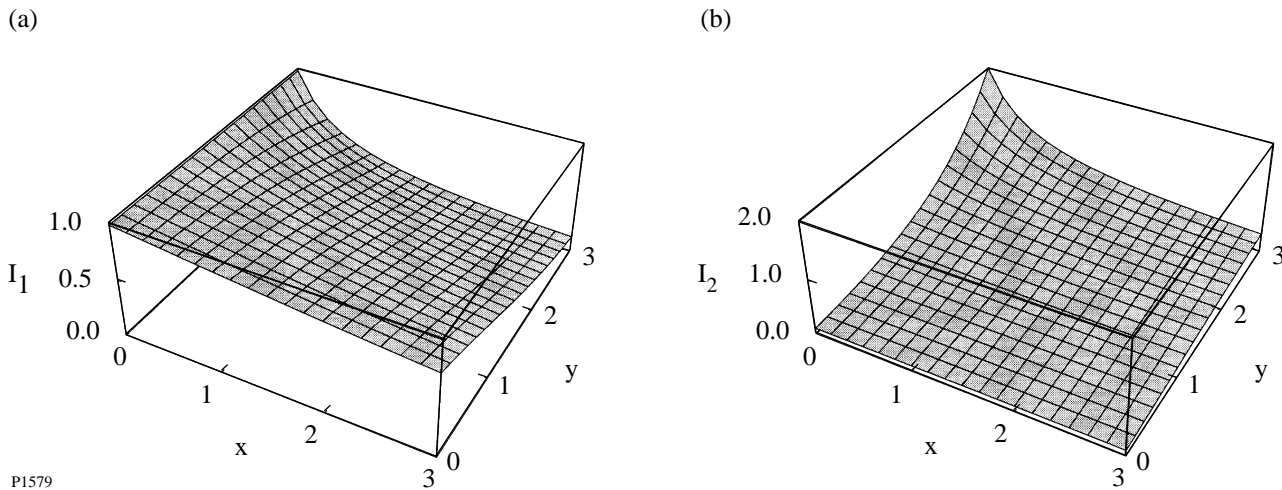
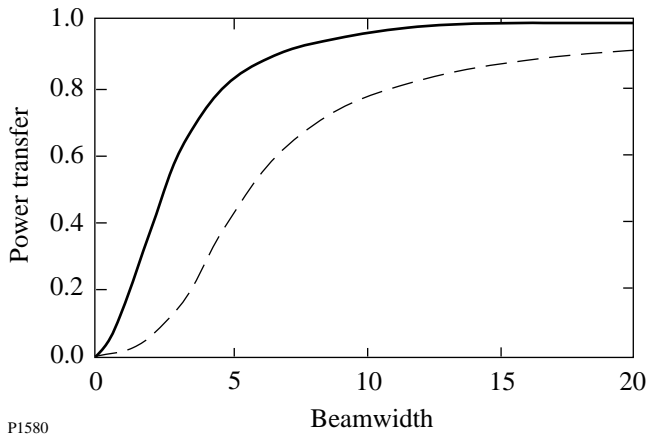


Figure 66.33 Beam-intensity profiles [Eqs. (18)] for the case in which the normalized beamwidth $l = 3$ and the ratio of the incident beam intensities $r = 0.1$. Notice that the intensity profiles are highly two-dimensional.



P1580

Figure 66.34

Fractional power transfer from beam 1 to beam 2 [Eq. (21)] plotted as a function of the normalized beamwidth l for two values of r , the ratio of the incident beam intensities. The dashed line corresponds to $r = 0.01$, and the solid line corresponds to $r = 0.1$.

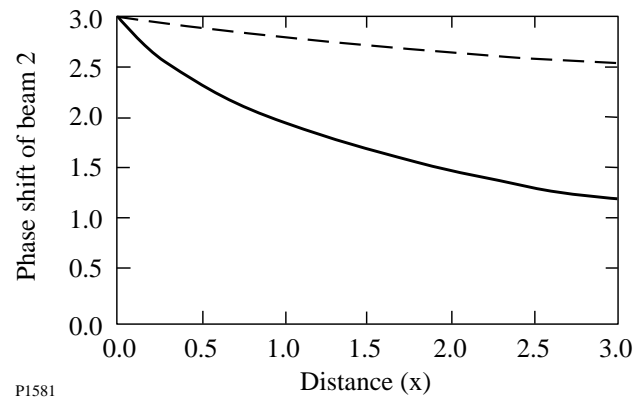
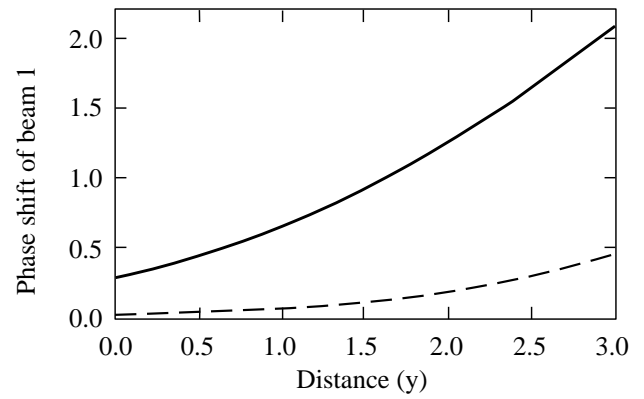
and the plasma. As a numerical example, suppose that the electron density $n_e = 10^{20} \text{ cm}^{-3}$, the electron temperature $T_e = 1 \text{ keV}$, the ion temperature $T_i = 0.5 \text{ keV}$, the laser wavelength $\lambda_0 = 0.35 \text{ }\mu\text{m}$, the laser intensity $I_0 = 10^{15} \text{ Wcm}^{-2}$ and the beamwidth $w = 1 \text{ mm}$. For these parameters $l \approx 2.7$. One can infer the value of l for other parameters by using the fact that, with the electron-to-ion temperature ratio fixed, l is proportional to $n_e \lambda_0 I_0 w$ and is inversely proportional to T_e .

Since Eq. (21) is valid for $0 < \theta < \pi$, the angular dependence of l is also of interest. When $\delta = 0$, $\beta |A_0|^2$ is the spatial growth rate of SBS. For an ion-acoustic wave subject to Landau damping, this growth rate is independent of θ .^{8,9} In this case, l is inversely proportional to $\sin \theta$: the power transfer is larger for beams that are nearly parallel or antiparallel because they overlap for a longer distance. The importance of $\delta \neq 0$ is measured relative to ω_s and v_s , both of which are proportional to $\sin(\theta/2)$. Thus, the power transfer is more sensitive to detuning when the beams are nearly parallel and less sensitive when the beams are nearly antiparallel.

When $\delta \neq 0$, the interaction of beams 1 and 2 causes their phases to be shifted by ϕ_1 and ϕ_2 , respectively. It follows from Eqs. (11) and (15) that

$$\phi_1(y) = \alpha P_2(l, y) / 2\beta I_0, \quad \phi_2(x) = \alpha P_1(x, l) / 2\beta I_0. \quad (22)$$

The normalized phase shifts $P_2(l, y)$ and $P_1(x, l)$ are plotted as functions of position in Fig. 66.35. An observer traveling with



P1581

Figure 66.35

Normalized phase shifts [Eqs. (22)] plotted as functions of position for the case in which the normalized beamwidth $l = 3$ and for two values of r , the ratio of the incident beam intensities. The dashed lines correspond to $r = 0.01$, and the solid lines correspond to $r = 0.1$. The spatial inhomogeneity of these phase shifts causes the beams to be deflected.

either beam would measure a larger normalized phase shift on the left side of the beam.

For beams of moderate width ($l \sim 1$), the variation of phase with distance is approximately linear and the beam deflection angles θ_1 and θ_2 are easily estimated. It follows from the laws of geometrical optics that

$$\theta_1 \approx [\phi_1(l) - \phi_1(0)] / k_1 w, \quad \theta_2 \approx [\phi_2(0) - \phi_2(l)] / k_2 w. \quad (23)$$

By combining Eqs. (22) and (23), and neglecting the difference between k_1 and k_2 , one can show that

$$\theta_1 \approx \theta_2 \approx (\alpha / k_2 \sin \theta) [T(l) / l]. \quad (24)$$

Both beams are deflected in the same angular direction: anticlockwise when $\delta < 0$ and clockwise when $\delta > 0$. Because the fractional power transfer depends on l and, hence, on β , the beam deflection angle [Eq. (24)] depends on both α and β . It is evident from Fig. 66.31 that the magnitude of the beam deflection angle is largest when $|\delta| \sim v_s$. When $\delta = 0$ or $\delta = -\omega_s$, the beams are not deflected.

For wide beams ($l \gg 1$) the phase of beam 1 still varies approximately linearly with distance and the first of Eqs. (24) is still valid. Unfortunately, the variation with distance of the phase of beam 2 is highly nonlinear, and it is difficult to estimate the beam deflection angle and focusing distance. In this case, however, the power transfer from beam 1 to beam 2 is complete: the irradiation symmetry is destroyed and the issues of beam deflection and focusing are irrelevant.

The beam deflection angle is larger for beams that are nearly parallel or antiparallel because the nonlinear phase shifts that deflect the beams are proportional to the power transfer. For the same reason, the beam deflection angle is more sensitive to detuning when the beams are nearly parallel and less sensitive to detuning when the beams are nearly antiparallel.

Transient Analysis

Equations (18) and (21) describe completely the steady-state power transfer between beams 1 and 2. However, it is important to know how long the beam interaction takes to reach steady state. If this saturation time is comparable to the duration of the interaction, the transient power transfer must also be determined.

The case in which $\delta = -\omega_s$ has been studied theoretically and experimentally.^{10,11} In steady state, beam 2 is unamplified. However, the response of the ion-acoustic wave to a steady ponderomotive force includes a resonant transient that is required to satisfy the initial conditions. This resonant response produces a frequency-downshifted component of beam 2. In turn, the frequency-downshifted component of beam 2 gives rise to a component of the ponderomotive force that drives the ion-acoustic wave resonantly. Because of this feedback mechanism, the transient (SBS) grows considerably and lasts for a time that is long compared to the damping time of the ion-acoustic wave.

We consider here the complimentary case in which $|\delta| \ll \omega_s$, and the linearized equations can be simplified and solved exactly. It is advantageous to work in terms of the ion-acoustic amplitude

$$N(\xi, \eta, t) = n(\xi, \eta, t) \exp(i\omega t), \quad (25)$$

which satisfies the simplified equation

$$(\partial_t + v_s - i\delta)N = -i(\omega_s A_0/2)A_2^*. \quad (26)$$

Subject to the normalized boundary and initial conditions

$$A_2(0, \eta, t) = 1, \quad A_2(\xi, \eta, 0) = 1, \quad (27)$$

which differ from the physical conditions by a factor of ρA_0 , and the initial condition

$$N(\xi, \eta, 0) = 0, \quad (28)$$

the solution of Eq. (26) and the second of Eqs. (5) is

$$A_2(\eta, t) = 1 + \gamma \int_0^t (\eta/v_2 t)^{1/2} I_1 \left[2\gamma(\eta t'/v_2)^{1/2} \right] \times \exp[-(v_s - i\delta)t'] dt', \quad (29)$$

$$N(\eta, t) = -i(\omega_s A_0/2) \int_0^t I_0 \left[2\gamma(\eta t'/v_2)^{1/2} \right] \times \exp[-(v_s - i\delta)t'] dt',$$

where

$$\gamma = \left(\omega_e^2 \omega_s^2 |A_0|^2 / 4\omega_2 \omega_s \right)^{1/2} \quad (30)$$

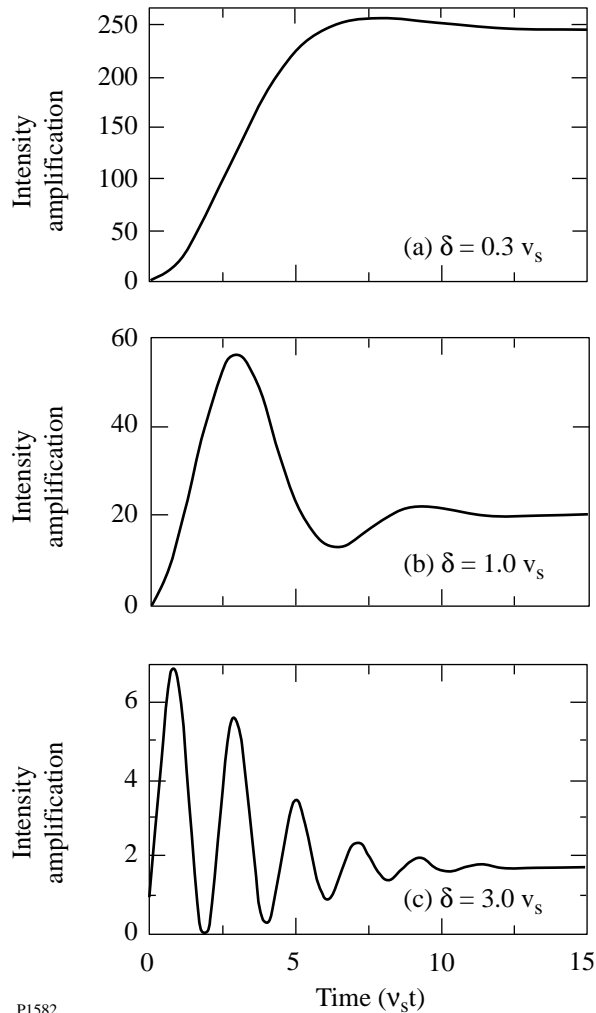
is the temporal growth rate of SBS in an infinite plasma and I_m denotes a modified Bessel function of the first kind, of order m (rather than a beam intensity). It is evident from this solution that the linear evolution of beam 2 is one-dimensional. As $t \rightarrow \infty$,

$$A_2(\eta, t) \rightarrow \exp[\gamma^2 \eta / v_2 (v_s - i\delta)], \quad (31)$$

$$N(\eta, t) \rightarrow -[i\omega_s A_0/2(v_s - i\delta)] \exp[\gamma^2 \eta / v_2 (v_s - i\delta)],$$

in agreement with the linearized versions of Eqs. (13).

The normalized intensity of beam 2 is plotted as a function of $v_s t$ in Fig. 66.36 for the case in which the spatial growth parameter $\gamma^2 \eta / v_2 v_s = 3$ and for three values of δ . The oscil-



P1582

Figure 66.36
Intensity amplification of beam 2 [which follows from the first of Eqs. (29)] plotted as a function of $v_s t$ for the case in which the spatial growth parameter $\gamma^2 \eta / v_2 v_s = 3$. (a) $\delta = 0.3 v_s$; (b) $\delta = 1.0 v_s$; (c) $\delta = 3.0 v_s$.

lations in beam intensity are due to the beating of the driven response and the resonant transient. As the magnitude of δ increases, the maximal transient intensity decreases less than the steady-state intensity, so the transient becomes more important. For the case in which $\delta = 0$, the linear saturation time is^{8,9}

$$t_s \approx 2\gamma^2 \eta / v_2 v_s^2. \quad (32)$$

When $\delta \neq 0$, some oscillations persist for a longer time, but the beam intensity is of the order of the steady-state intensity at this time: the saturation time does not depend sensitively on δ and is well approximated by Eq. (32).

For a fixed value of η , the saturation time is inversely proportional to $\sin(\theta/2)$.^{8,9} However, in the present context, the maximal value of η is $w/\sin\theta$ and the saturation time is inversely proportional to $\sin\theta \sin(\theta/2)$. Thus, the saturation time is longer for beams that are nearly parallel or antiparallel, and the increase in saturation time is larger for beams that are nearly parallel.

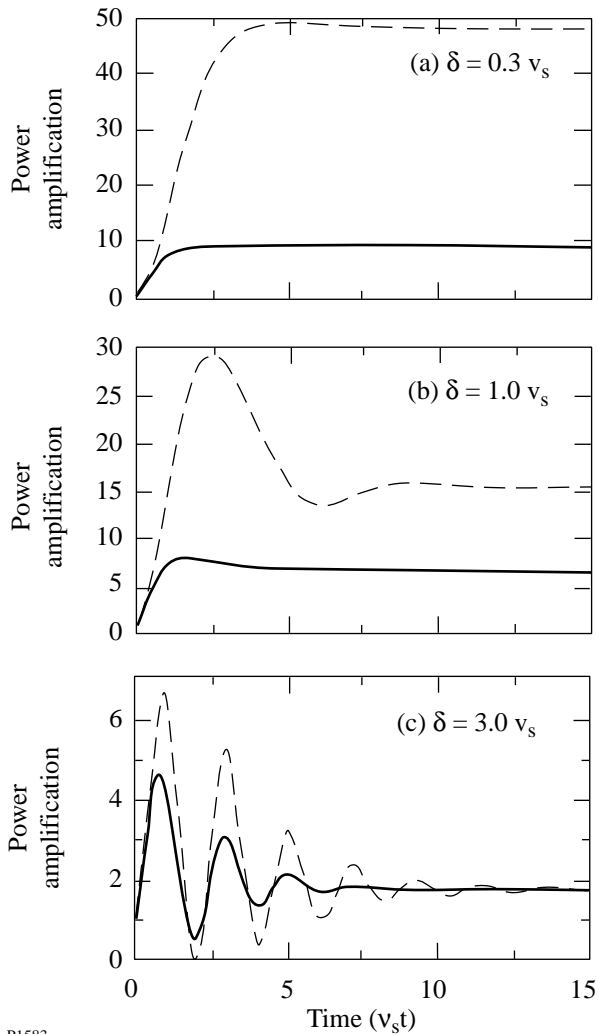
It is evident from Figs. 66.32 and 66.33 that two-dimensional evolution signifies the convective depletion of beam 1, which is a nonlinear effect. When the beams are only moderately wide or the ratio of the incident beam intensities is small, the steady-state interaction of the beams is approximately one-dimensional and is consistent with the linearized Eqs. (31). For these cases we expect the transient evolution of the beams to be well described by Eqs. (29). However, when the beams are wide or the incident intensities are comparable, the depletion of beam 1 is significant and the nonlinear Eqs. (5) and (26) must be used to determine the transient evolution of the beams.

Numerical Simulations

Equations (5) and (26) were solved numerically, and the total power passing through the exit boundary of each beam was determined as a function of time. The power amplification of beam 2 is plotted as a function of $v_s t$ in Fig. 66.37 for the case in which $\gamma^2 \eta / v_2 v_s = 3$ and for three values of δ . The dashed line corresponds to $r = 0.01$, for which the maximal amplification is 101, and the solid line corresponds to $r = 0.1$, for which the maximal amplification is 11. Although plotting the power amplification rather than the absolute power transfer disguises the fact that $T(l)/l \leq 1$, it facilitates a comparison of the analytical and numerical results. In particular, the deviation of the two numerical curves from one another signals the onset of nonlinearity.

By comparing Figs. 66.36 and 66.37 one notes that when $r = 0.01$, the predictions of linear theory are quantitatively correct for $\delta = 3.0 v_s$ and qualitatively correct for $\delta = 1.0 v_s$ and $\delta = 0.3 v_s$. When $r = 0.1$, the predictions of linear theory are qualitatively correct for $\delta = 3.0 v_s$ and incorrect for $\delta = 1.0 v_s$ and $\delta = 0.3 v_s$. The numerical results show that the onset of nonlinearity is more rapid, and its effect on the transient and steady-state power amplification is more dramatic when the incident intensity of beam 2 is high or the normalized beam width is large [see the second of Eqs. (8) and (9), and Fig. 66.31].

When nonlinearity is important, the interaction saturates more quickly than linear theory predicts. The extent to which



P1583

Figure 66.37

Power amplification of beam 2 plotted as a function of $v_s t$ for the case in which the spatial growth parameter $\gamma^2 \eta / v_2 v_s = 3$. The power amplification was determined numerically for two values of r , the ratio of the incident beam powers. The dashed line corresponds to $r = 0.01$, for which the maximal amplification is 101, and the solid line corresponds to $r = 0.1$, for which the maximal amplification is 11. (a) $\delta = 0.3 v_s$; (b) $\delta = 1.0 v_s$; (c) $\delta = 3.0 v_s$.

beam 1 is depleted changes in the time taken for the beams to cross the interaction region. In the model Eqs. (5) and (26) this transit time is instantaneous. Thus, the depletion of beam 1 allows both beam intensities to adjust to their steady-state profiles on a time scale that is short compared to the damping time scale inherent in linear theory.

Nonlinearity becomes important when $2\gamma(\eta t / v_2)^{1/2}$, the argument of the amplifying terms in Eqs. (29), reaches a critical value that is inversely dependent on r . It follows from

this condition that the nonlinear saturation time is inversely proportional to $\gamma^2 \eta$. For fixed η , the nonlinear saturation time is inversely proportional to $\sin(\theta/2)$, as is the linear saturation time [Eq. (32)]. However, in the present context the maximal value of η is $w/\sin\theta$ and the nonlinear saturation time is proportional to $\cos(\theta/2)$.

Summary

The power transfer between crossed laser beams made possible by an ion-acoustic wave was studied in detail. Despite the complexity of the beam evolution, which is two-dimensional and nonlinear, a simple formula was derived for the steady-state power transfer. This power transfer depends on two dimensionless parameters: the ratio of the incident beam intensities and the normalized beamwidth. The normalized beamwidth is proportional to the physical beamwidth and the intensity of the higher-frequency beam, and is inversely dependent on the detuning of the laser difference frequency from the ion-acoustic frequency. Numerical simulations showed that the transient power transfer is larger than the steady-state power transfer and usually oscillates in time. The convective depletion of the higher-frequency beam saturates the power transfer more quickly than the damping of the ion-acoustic wave. The deflection of each beam by the other was also studied briefly.

The analysis of this article is based on the standard model² in which the beams are assumed to be monochromatic and their interaction is assumed to be in steady state. This simplified model allows one to understand the basic physics of the power transfer from the higher-frequency beam to the lower-frequency beam. A more realistic model¹ would allow the beams to have many frequency components. The analysis of such a model, in both the transient and steady-state regimes, will be the subject of future work.

ACKNOWLEDGMENT

This work was supported by the National Science Foundation under Contract No. PHY-9057093, the U.S. Department of Energy (DOE) under Contract No. W-7405-ENG-36, the U.S. Department of Energy Office of Inertial Confinement Fusion under Cooperative Agreement No. DE-FC03-92SF19460, the University of Rochester, and the New York State Energy Research and Development Authority. The support of DOE does not constitute an endorsement by DOE of the views expressed in this article.

REFERENCES

1. J. D. Lindl, *Phys. Plasmas* **2**, 3933 (1995).
2. W. L. Kruer *et al.*, *Phys. Plasmas* **3**, 382 (1996).

3. V. V. Eliseev, W. Rozmus, V. T. Tikhonchuk, and C. E. Capjack, "Interaction of Crossed Laser Beams with Plasmas," to be published in *Physics of Plasmas*.
4. W. L. Kruer, *The Physics of Laser Plasma Interactions*, Frontiers in Physics, Vol. 73 (Addison-Wesley, Redwood City, CA, 1988), Chaps. 7 and 8.
5. The normalized action flux amplitudes A_1 and $(\omega_2 v_2 / \omega_1 v_1)^{1/2} A_2$ satisfy Eqs. (7) exactly.
6. M. Maier, W. Kaiser, and J. A. Giordmaine, *Phys. Rev.* **177**, 580 (1969).
7. T. Speziale, *Phys. Fluids* **27**, 2583 (1984).
8. C. J. McKinstrie, R. Betti, R. E. Giacone, T. Kolber, and J. S. Li, *Phys. Rev. E* **50**, 2182 (1994).
9. R. E. Giacone, C. J. McKinstrie, and R. Betti, *Phys. Plasmas* **2**, 4596 (1995).
10. J. S. Li, C. J. McKinstrie, C. Joshi, and K. Marsh, *Bull. Am. Phys. Soc.* **39**, 1584 (1994).
11. K. Marsh, C. Joshi, and C. McKinstrie, *Bull. Am. Phys. Soc.* **39**, 1585 (1994).